Shaping reverberating sound fields with an actively tunable metasurface

Guancong Ma[a,b,c,1,2], Xiying Fan[b,1,3], Ping Sheng[a,b,2], and Mathias Fink[a,d,2]

[a]Institute for Advanced Study, Hong Kong University of Science and Technology, Clear Water Bay, Kowloon, Hong Kong; [b]Department of Physics, Hong Kong University of Science and Technology, Clear Water Bay, Kowloon, Hong Kong; [c]Department of Physics, Hong Kong Baptist University, Kowloon Tong, Hong Kong; and [d]Institut Langevin, CNRS, École supérieure de physique et de chimie industrielles de la Ville de Paris, Université Paris Sciences & Lettres, 75005 Paris, France

Edited by John B. Pendry, Imperial College London, London, United Kingdom, and approved May 15, 2018 (received for review January 22, 2018)

A reverberating environment is a common complex medium for airborne sound, with familiar examples such as music halls and lecture theaters. The complexity of reverberating sound fields has hindered their meaningful control. Here, by combining acoustic metasurface and adaptive wavefield shaping, we demonstrate the versatile control of reverberating sound fields in a room. This is achieved through the design and the realization of a binary phase-modulating spatial sound modulator that is based on an actively reconfigurable acoustic metasurface. We demonstrate useful functionalities including the creation of quiet zones and hotspots in a typical reverberating environment.

acoustics | reverberation | metasurface | wavefront shaping

Wave control is a challenging task in complex media, wherein waves are scrambled by multiple scatterings (1). Over the last decade, optical adaptive wavefront shaping has become an impressive tool to control light propagation through highly scattering systems (2, 3). These advances have largely been enabled by the availability of highly tunable digital arrays, known as spatial light modulators. They allow us to synthesize a wavefront matched to a specific diffusive medium to achieve functionalities such as focusing through turbid media (4–6), noninvasive imaging (7–10), holography (11), etc. This strategy was also developed recently in microwaves for wireless communications (12–14). As an important class of complex media, reverberating environments are commonplace for airborne sound. Most indoor environments are reverberating acoustic cavities. A sound from any source is multiple-scattered by boundaries (walls, ceiling, and floor) and objects (furniture, warm bodies, etc.), forming a 3D complex wavefield (15) that is similar to laser speckles. The control of sound in such rooms is therefore an extremely challenging yet useful topic. Here, we propose an approach based on wavefront shaping. We demonstrate the active shaping of any reverberating sound field by introducing a spatial sound modulator (SSM) that is a reconfigurable acoustic metasurface acting as an array of binary phase modulators. The SSM, which has the lateral dimension of several wavelengths and only covers a small fraction of the total surface area of the room, can drastically alter the sound field, while the source and the room remain unchanged. Experiments show the successful creation of "quiet zones" as well as an "acoustic hotspot" in a reverberating room. With this method, the reverberation of a room is no longer a constraint but becomes a tunable property.

We conducted the investigation in our laboratory, which is approximately a cuboid acoustic cavity. At the reverberating regime, the interference of the rich eigenmodes in the room gives rise to a complex, disordered sound field (15). Various furniture and equipment pieces inside the laboratory introduce multiple scatterings that further scramble the sound. This can be seen in Fig. 1*A*, which shows a collection of simulated fields for a cuboid cavity that is the similar size and shape of the laboratory. Over 30 eigenmodes are found within 600–601 Hz. [This is also known as the modal overlap factor (16).] How to achieve meaningful control of such a complex sound is our main goal. Owing to the room's finite quality factor, each mode has a certain degree of spectral broadening, so that a monochromatic sound can excite all modes within a frequency correlation bandwidth of ∼5 Hz. (See *Materials and Methods* for more details about the testing environment.) Since these eigenmodes are essentially standing waves, we can alter their interference by binary phase modulation, which means to encode a specific set of phase factors of 0 or π to a sufficient number of modes. The idea is schematically shown in Fig. 1*B*, wherein each arrow represents a mode's contribution to the local field in the form of $P = P_0 e^{i\phi}$. The length of the arrow is the amplitude P_0, and the arrow's direction is determined by the phase ϕ. Naturally, the total local field (black arrow) is the sum of all arrows. Adding a phase factor of π to a mode means inverting the direction of the corresponding arrow. Meaningful control of local field is possible if only a portion of the modes (red arrows) is sensitive to phase modulation. For example, as shown in Fig. 1*B*, the objective to obtain minimum pressure amplitude, i.e., locally suppress the sound intensity by destructive interference, is achieved by inverting only two arrows labeled 1, 3.

Design of Actively Tunable Metasurface

The core of such functionality is a phase modulator comprising an array of pixels, each capable of bestowing the transmitted or reflected waves with a desirable phase factor. In this work, we choose to work with the transmitted waves. In optics, spatial light modulators are commercially available. However, no equivalent

Significance

Wavefront shaping with spatial light modulators has recently motivated many studies in the field of light manipulation in diffusive media. Here, we extend this concept to acoustic waves by designing and building a binary phase-modulating spatial sound modulator (SSM). The SSM is an acoustic metasurface consisting of unit cells with two states, switchable through programmed electronics. We demonstrate in audible frequencies, and in a reverberating environment, the capability of controlling and reshaping any complex sound field. Our work will not only open avenues to study wave propagation in complex and chaotic media but also inspire applications in acoustic engineering.

Author contributions: G.M. and M.F. designed research; G.M. and X.F. performed research; G.M., X.F., P.S., and M.F. analyzed data; and G.M., P.S., and M.F. wrote the paper.

The authors declare no conflict of interest.

This article is a PNAS Direct Submission.

[1]G.M. and X.F. contributed equally to this work.

[2]To whom correspondence may be addressed. Email: phgcma@hkbu.edu.hk, sheng@ust.hk, or mathias.fink@espci.fr.

[3]Present address: School of Physics and Technology, Wuhan University, Wuhan 430072, China.

This article contains supporting information online at www.pnas.org/lookup/suppl/doi:10.1073/pnas.1801175115/-/DCSupplemental.

Published online June 11, 2018.

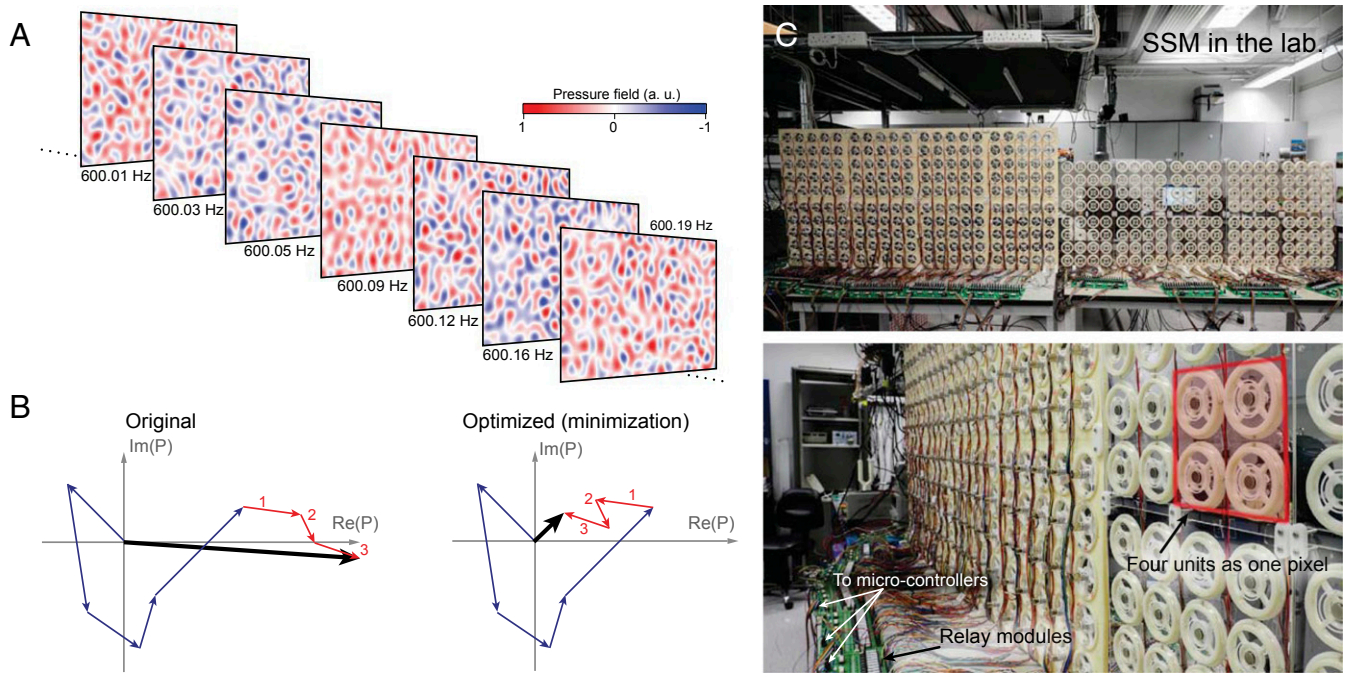

Fig. 1. A collection of simulated eigenmodes of a cavity of similar size and shape with our laboratory is shown in *A*. These modes constitute the degree of freedom for controlling reverberating sound via SSM. The control concept is shown in *B*. Each arrow is a complex number that represents a mode's contribution to the local field. Blue arrows represent modes unaffected by SSM's modulation. Red arrows are modes sensitive to the modulation. In binary phase modulation, to obtain the smallest total field (shortest black arrow), two arrows labeled 1, 3 are inverted, which means picking up a phase factor of π. Photos in *C* show the SSM, which consists totally 360 units of binary active MRs. Four units are grouped together as one pixel, each being electrically controlled by programmable electronics.

device exists for airborne sound. Moreover, the inherently long wavelength of airborne sound presents an additional challenge for phase manipulation within a small device. The recent advent of acoustic planar metamaterials/metasurfaces (17–19) offers a potential solution for such a task. Since the existing acoustic metasurfaces are not actively reconfigurable, we have designed and realized an actively reconfigurable acoustic metasurface that can play the crucial role of a deep-subwavelength, phase-modulating binary spatial sound modulator (SSM).

The SSM is based on membrane-type resonators (MRs) that have been studied in previous works (20–24). The MR resonates under the excitation of subkilohertz airborne sound; each of its resonances can introduce (in the absence of dissipation) a phase change of π in the transmitted wave. If we can actively shift a resonance between two frequencies, a phase factor of either 0 or π can be attained for transmitted sound in the intermediate frequency range, thereby leading to binary phase modulation (12, 25).

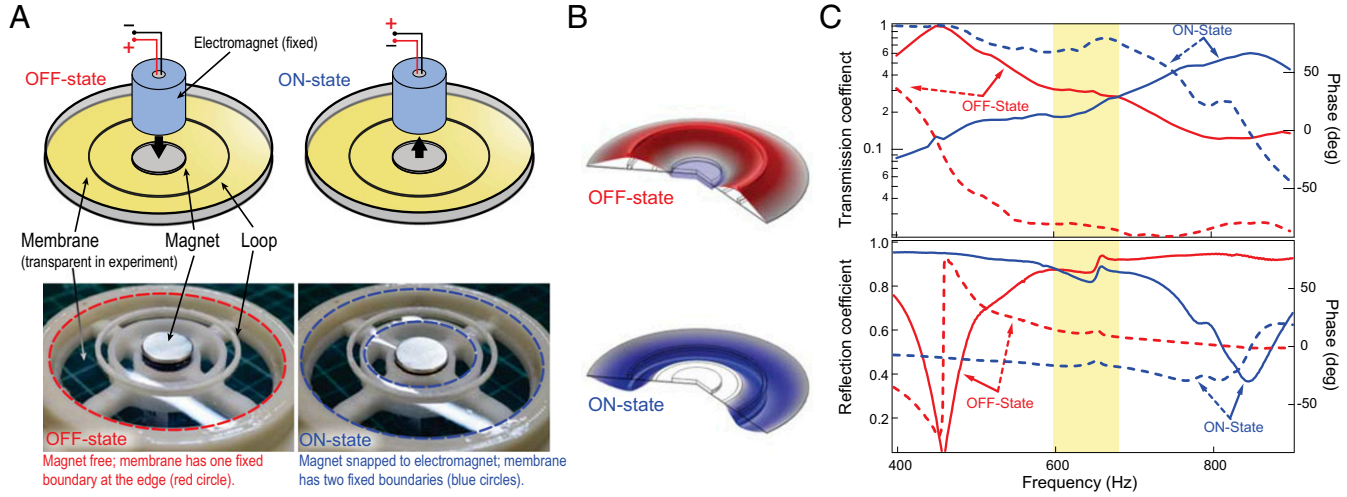

Fig. 2. The unit cell design is shown in *A*. The membrane can be electrically switched between two states, one (denoted OFF state) has one fixed boundary at its edge; the other (denoted ON state) has two fixed boundaries. State switching is achieved by switching the polarity of the dc voltage across the electromagnet. Simulated vibration profiles of the two states are shown in *B*. Measured transmission, reflection coefficients (solid curves), and their phases (dashed curves) of an MR at both states are shown in *C*. In the frequency regime of 600–680 Hz (shaded yellow), the two states have a phase difference of ~150° in the transmitted waves. However, the amplitude of transmission and reflection coefficients and the reflection phase remain similar.

The unit cell designed to achieve the above function is shown in Fig. 2*A*. A circular elastic membrane is stretched and fixed at the edge. A small magnet disk and a plastic loop are attached to the membrane as loaded mass to tune its eigenmodes. A resonance is identified as a transmission peak at 450 Hz (Fig. 2*C*, red). To make the unit cell actively tunable, we place a small electromagnet directly above the magnet disk, separated by a small gap, as depicted in Fig. 2*A*. By applying a dc voltage, the electromagnet can firmly snap the magnet disk to stop the vibration of the inner part of the membrane. This imposes an additional fixed boundary within the membrane, effectively turning the circular membrane into an annular one, as shown in Fig. 2*A*. We denote this as the unit's "ON state." Inverting the dc voltage changes the polarity of the electromagnet and releases the MR to its original state, which we denote as "OFF state." This change of the MR significantly impacts its eigenmodes, as shown in the vibration profiles in Fig. 2*B*. Notably, the resonant peak at the OFF state near 450 Hz is shifted to 850 Hz at the ON state (Fig. 2*C*). In the frequency regime of 600–680 Hz, we observe that the MR at its two switchable states has a phase difference of ∼150° in the transmitted waves, but the amplitude of transmission and reflection coefficients, as well as phases of the reflected waves, remain at a similar level. This property is suitable for a binary phase-modulating SSM.

We have fabricated a metasurface comprising 360 identical units of MRs in a 2D array (Fig. 1*C*). The array has a total area of 2.3 m^2, which is less than 1% of the laboratory's total boundary area. The lateral dimension of the MRs is subwavelength and is therefore not desirable for controlling the far field. We mitigate this problem by grouping four units into a 2×2 array to form one functional pixel. With each MR unit controlled by programmable electronics, the metasurface becomes an SSM that has a total of 90 pixels.

Active Shaping of Reverberating Sound Fields

We demonstrate the SSM's capability in controlling reverberating sound by creating quiet zones at a particular position in our laboratory. To achieve this, the SSM has to minimize the sound level at a particular position for a specific frequency. Similar to optical wavefront shaping, the SSM must communicate with a sensor through a feedback loop. We place a small microphone at the chosen position to measure the sound amplitude *P*, and use it as the feedback to guide the optimization of the SSM. We use a simple iterative optimization scheme (4, 26), *viz*., we compare the measured pressure at the chosen position for each pixel at both of its states, and keep the pixel at the state that yields a smaller *P*. The process is repeated for all pixels. A typical result is shown in Fig. 3 *A* and *B*. At the chosen frequency of 636 Hz, the SSM

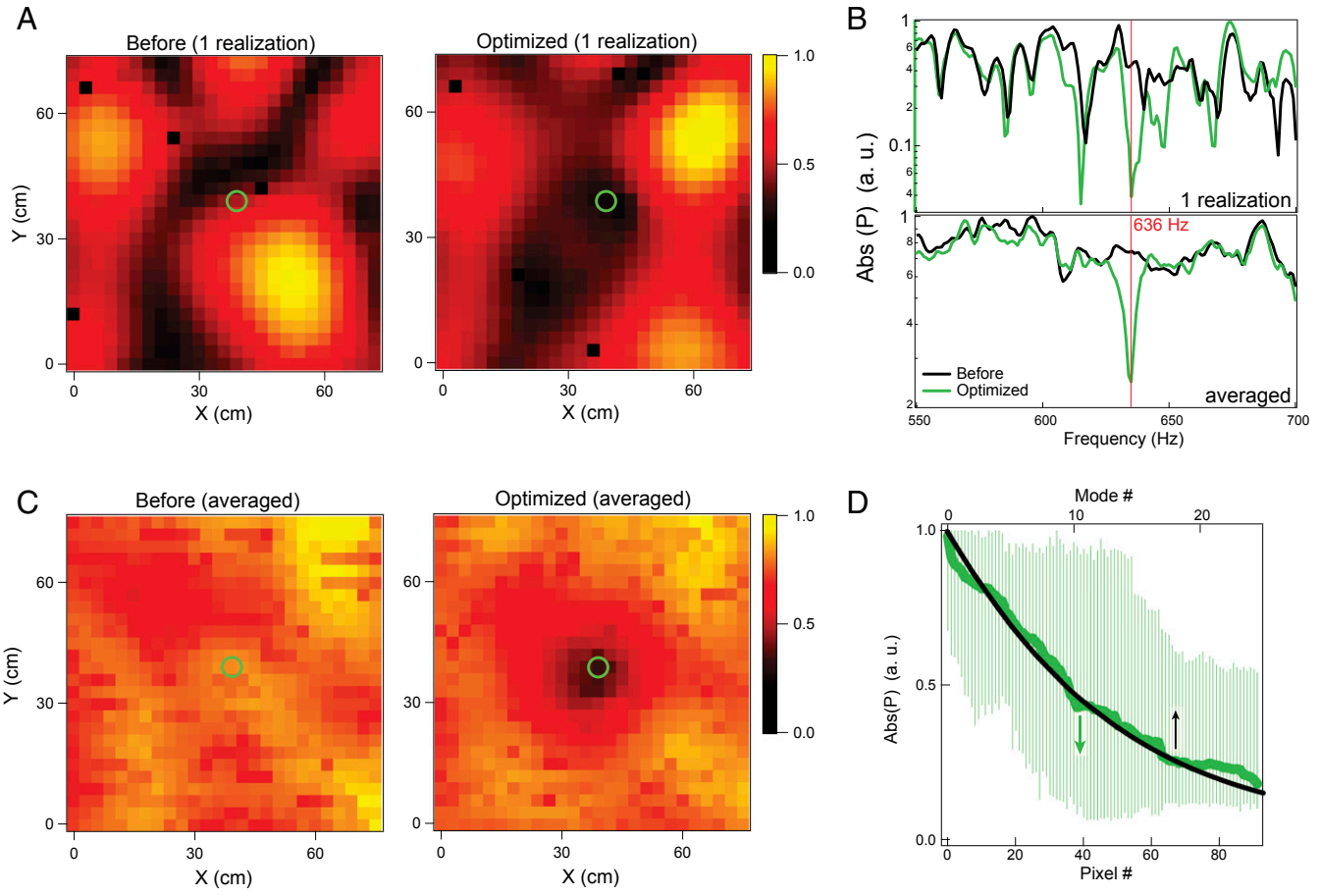

Fig. 3. The SSM is used to minimize the acoustic pressure amplitude at 636 Hz at the position that is marked by the green circle. A typical realization is shown in *A*. It is seen that despite the complexity, the SSM can alter the field pattern by modulating the phases of a sufficient number of the modes so that a local minimum is created at the chosen position. For this specific case, the sound intensity is reduced by 21 dB, as also shown in the pressure spectra in *B* (*Upper*). (*B*, *Lower*) Pressure spectra averaged over 35 realizations at uncorrelated positions. (*C*) Average field of all 35 realizations, wherein a zone of low acoustic pressure clearly emerges after optimization. Meanwhile, the complex fields even out in the same averaging process. Optimization histories averaged over all 35 realizations are plotted as green curve in *D* (bottom axis), wherein error bars are determined by 35 individual realizations. The black curve in *D* is from the optimization model, with sound amplitude plotted as a function of modes being controlled (top axis). Colors in *A* and *C* represent pressure amplitude.

reduces the sound intensity by 21 dB (Fig. 3*B*). We further obtain spatial maps of the sound fields before and after optimization, as shown in Fig. 3*A*. First, we see that field patterns in both cases are disordered, which conforms with the complex characteristics of reverberating sound. Despite such complexity, we clearly see that a region of small sound pressure emerges at the optimization position, which is marked by the green circle.

We have further performed 35 independent minimization experiments for 636 Hz at uncorrelated positions in the laboratory. In Fig. 3*C* we show the averaged field patterns of all 35 experiments. It is seen that the preoptimized field has relatively uniform distribution after averaging, which is yet another evidence of the disordered characteristic of reverberating sound. The optimized field, however, clearly shows a diffraction-limited zone of smaller sound pressure at the optimized position. Also, from the averaged frequency response at the optimized positions (Fig. 3*B*), we can see that P is significantly reduced near 636 Hz. In addition, the minimization histories averaged over all 35 experiments are shown in Fig. 3*D*. We can clearly see that as each pixel's state is sequentially determined, P indeed steadily decreases throughout the process. This is further evidence of the effectiveness of the SSM. The minimization process can be reproduced with a simple numerical model (details are presented in *Materials and Methods*). The result from the model is also shown in Fig. 3*D*. Excellent agreement is seen. On average, the minimization can reduce the sound intensity by 11 dB. We also demonstrate the quiet zone in Movie S1.

Similarly, by using an optimization criterion to keep the pixels' states that yield a larger sound level, the SSM can achieve the opposite and can generate an acoustic hotspot. We show the results in Fig. 4.

Discussion

By combining metamaterials and wavefield shaping, we have successfully realized an SSM to harness the degrees of freedom that underlie reverberating sound, and have demonstrated actively reconfigurable control of local sound intensity. The optimization of sound field can be easily modeled using random numbers. Details of the model are presented in *Materials and Methods*. The results are plotted as black curves in Fig. 3*D* (for minimization) and in Fig. 4*D* (for maximization). Here, the horizontal axes (top axes) are the number of the room's modes under control by the SSM. (This is different from the pixel number on the SSM.) It is seen that by controlling only 25 modes, good agreement with experiments can be achieved. The discrepancy in Fig. 4*D* is mainly attributed to the relatively small number of experimental realizations.

The SSM's capability in sound-field control goes far beyond traditional wisdom. Reverberation has been widely regarded as an intrinsic property of a room. Its complexity also makes refined

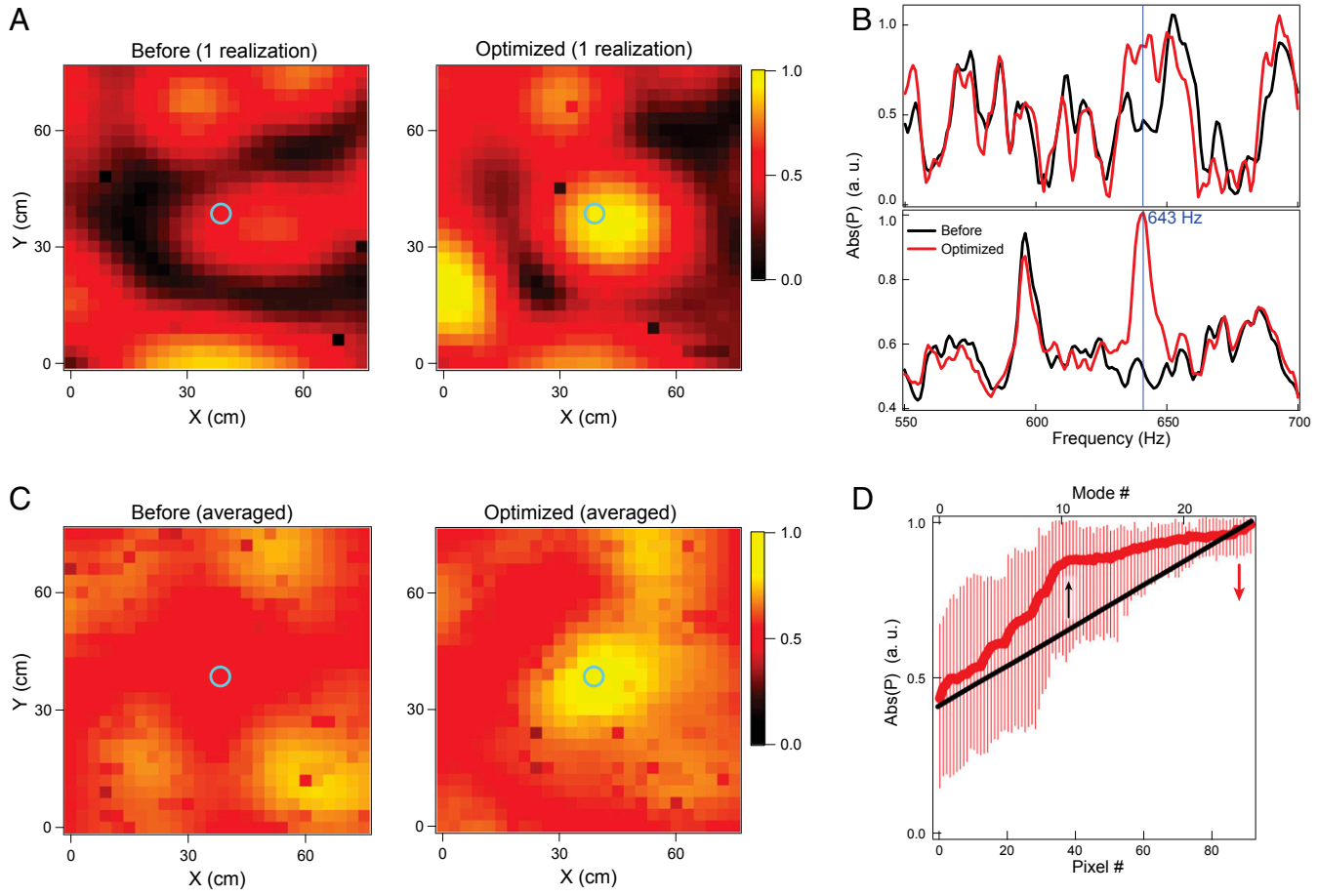

Fig. 4. The SSM is used to maximize the acoustic pressure amplitude at 643 Hz at the position that is marked by the cyan circle. A typical realization is shown in *A*, in which the SSM creates a local maximum. The pressure spectra at the optimized position are shown in *B* (*Upper*). (*B*, *Lower*) Pressure spectra averaged over 25 realizations at uncorrelated positions. (*C*) Average field for these 25 realizations, in which high acoustic pressure at the optimized position is clearly observed in the optimized field. (*D*) The red curve is the experimental optimization process averaged over 25 realizations as a function of pixel number (bottom axis). Error bars in *D* are given by individual optimization histories. The black curve in *D* is from the theoretical model (top axis). Colors in *A* and *C* represent pressure amplitude.

control extremely difficult. Its alteration usually requires an overhaul of the interior design. The creation of quiet zones anywhere in a room has the application value as a versatile noise abatement solution. Acoustic hotspots will be useful to improve audio quality, which may benefit music experience, oral communications, etc. In addition to these local modifications, the way SSM redistributes existing acoustic energy may even affect the global acoustic properties of the environment. For example, maximizing sound intensity at a position with localized high absorption can lead to the reduction of average sound level in the room, which is similar to coherent enhanced absorption (27).

We further point out that the way the SSM rearranges the distribution of the acoustic energy is fundamentally different from existing methods of active sound control, which demand additional source components that emit sound waves with the proper phase to cancel the sound field at the designated position (28), or to improve absorption performance (28–30). In comparison, the SSM consumes almost no energy unless the pixels are switching. The instability issues in active sound control, such as those caused by feedback time lag or phase errors, are nonexistent in our approach.

The sound-field control demonstrated in this paper is narrowband. However, such characteristic is mainly due to the optimization scheme, wherein the sound amplitude of a single frequency is used for feedback. Broadband control is also possible since the SSM can control the phases for modes in a much broader frequency regime (Fig. 2*C*). We show some results of broadband control in *SI Appendix*, Fig. S1. It is possible to further improve the performance by unit cell design. Since the MRs are highly tunable in their resonant frequencies, the SSM's bandwidth can be straightforwardly increased by combining MRs with mismatching resonant frequencies into supercells to act as pixel units. Also, smarter, more efficient optimization schemes can also play an important role in broadband control.

On the other hand, an SSM that modulates the amplitude or the phase of reflected waves may be a worthy goal for future development, since it can be integrated as a part of the boundary wall of the room.

Materials and Methods

The Design of the SSM. The SSM consists of 360 units of MRs grouped into 90 pixels. For each MR unit, a polyurethane membrane (27 mm in radius and 0.1 mm in thickness) is uniformly stretched by 10% and then glued to a plastic frame. A neodymium magnet disk with a radius of 6 mm and a mass of 0.9 g is attached to the center of the membrane. A plastic loop (inner/outer radius of 16/17 mm, 0.15 g) is also attached to the membrane. The disk and the loop tune one of MR's eigenmodes to 450 Hz. A miniature electromagnet is suspended at 2.5 mm from the membrane by a rigid plastic support. Embodied in the plastic support is a ring-shaped plateau. A small gap of 1 mm separates the membrane from this plateau. The magnet disk on the membrane snaps to the electromagnet when a suction magnetic force is established by applying dc voltage. The change in the magnet's position deforms the membrane and brings it into tight contact with the plateau. The constraint of the magnetic force essentially enforces a second fixed boundary that is the edge of the ring-shaped plateau. The membrane inside of the plateau becomes stationary at the frequency range of interest. The MR in this state, which we denote ON state, essentially has an annular shape. Inverting the dc voltage across the electromagnet inverts the direction of magnetic force so that the magnet and the membrane are pushed away to restore their free position. The membrane therefore retains circular shape, and resumes its original state that is denoted OFF state.

To switch each unit cell through dc voltage of different polarity (±15 V), all electromagnets are individually connected to an electrical relay. The relay modules are further controlled by eight units of Arduino Mega 2560 microcontrollers, which are programmed by a PC.

The Testing Environment. The experiments are performed in our laboratory, which is roughly a cuboid room with a dimension of 9.0(L) × 6.0(W) × 4.5(H) m. It can be considered reverberating above the Schroeder frequency $f_s = 2{,}000\sqrt{T_{60}V^{-1}} \approx 108\text{Hz}$, wherein V is the room's volume and T_{60} is the room's reverberation time for a 60-dB decay, which is measured to be about 0.7 s. The SSM is placed upright in the laboratory to take advantage of the phase change in the transmitted waves. The source is an omnidirectional loudspeaker.

The laboratory, which is an enclosed acoustic cavity, is characterized by its eigenmodes and the quality factor. The finite quality factor determines that each resonance has a certain degree of spectral broadening. This means a monochromatic excitation at frequency f can excite a wealth of resonances that lie within a frequency correlation bandwidth f_{cor} [also called "correlation frequency" in some literature (2)]. For a cuboidal cavity that is the basic shape of the room, the number of eigenmodes is estimated to be (15)

$$n = \left(\frac{4\pi V}{c^3}f^2 + \frac{\pi S}{2c^2}f + \frac{L}{8c}\right)f_{cor},$$

where V is the volume of the cavity, S is the total area of all boundaries, L is the total length of all edges, and c is the speed of sound. n is also known as the modal overlap factor that is commonly used for noise control (16). f_{cor} is related to the quality factor and therefore the exponential decay time τ through $f_{cor} = Q^{-1}f = (\pi\tau)^{-1}$. We measured τ with the interrupted signal method (with a sinusoidal source at 636 Hz) at multiple locations in the laboratory and obtained $\tau \approx 0.06$ s, which gives $f_{cor} \approx 5$ Hz. Consequently, we have $n \approx 165$ at $f = 636$ Hz. These modes, essentially standing waves inside the cavity, become the spatial degrees of freedom that can be accessed by the SSM to reshape the sound field. Irregular geometric features and scattering objects further scramble the field in the laboratory.

Experimental Configurations. During testing, no preference was given to the relative positions among the source, the SSM, and the optimization point. Typical layouts are schematically illustrated in *SI Appendix*, Fig. S2. Independent sets of experiments were carried out at uncorrelated positions, which are more than half a wavelength apart. All possible configurations are included: the source and the optimization point can be on a different side or the same side of the SSM; they can be close [but larger than the reverberation radius (31), which is about 1 m] or far apart; there may or may not be a direct line of sight among them.

Modeling the Optimization. The optimization of sound field can be numerically modeled. Here, we observe that total field at any position at a given frequency is

$$P_t = \sum_{i=1}^{n} P_i e^{i\phi_i}.$$

P_i is the local amplitude of the ith cavity mode at the chosen position, ϕ_i is the corresponding phase factor. n is the modal overlap factor, which is 165 for our experiments. According to the randomness characteristics of the reverberating field, we can use computer-generated pseudorandom numbers to simulate the optimization process. The simulation strategy for minimization goes as follows. First, we construct $u_i = P_i e^{i\phi_i}$ using random numbers, wherein P_i is positive random numbers between $(0, 1)$, ϕ_i is random numbers lying between $(-\pi, \pi)$. There are in total 165 numbers for u_i, corresponding to the $n = 165$ in our experiments. Second, we randomly choose $\sigma \le n$ numbers from u_i, and alter the phase ϕ_i to $\phi_i + 0.8\pi$ for each u_i (corresponds to the ∼150° phase factor bestowed by a pixel in our experiments). Then, choose the phase that yields a smaller P_t. Physically, σ is the number of modes controlled by the SSM, so there must be $\sigma \le n$. Since the exact number of modes under control is unknown in our experiment, we treat σ as the only tuning parameter in our model. (It should be noted that although the SSM has 90 pixels, exactly how many modes it can control is unknown.) Then, we record P_t for every step and repeat the process multiple times. The results from this model are shown in Figs. 3*D* and 4*D*. The numerical results are then averaged over 1,000 realizations. The number of modes under control is $\sigma = 25$. Good agreement with experiment is achieved. Some discrepancies are attributed to the relatively small number of experimental realizations (especially for the maximization results which have fewer realizations).

Performance Analysis. Several factors limit the performance of the SSM. From the above analysis of the experimental environment, with only 90 pixels, our SSM is insufficient to fully control the modes in the room (13). In addition, nonideal transmission coefficients of ∼0.3 (Fig. 2*C*) are observed for the MR in the operational frequency regime, which directly diminishes the overall performance, since the SSM only imprints phase factors to the transmitted waves. (This is why

the red arrows in Fig. 1*B* are shorter, which means smaller amplitudes.) Moreover, the inevitable dissipation associated with the MR slightly diminishes the phase change to ∼150°, instead of 180° that is the ideal value. This explains that in the averaged results (Fig. 3 *B* and *C*), the nonzero amplitude is seen at the minimization position, indicating imperfect destructive interference. To overcome these factors will be a goal of future studies.

With a continuous monochromatic excitation, our iterative method takes less than 9 min to complete the optimization for all pixels. Many viable paths can improve this performance. Smarter optimization methods such as genetic algorithm, machine-learning, etc., are good candidates to reduce the runtime. Prior knowledge of the environment and the sound field can also be integrated into the algorithm for better performance.

ACKNOWLEDGMENTS. We thank Yue Xiao and Shuyu Chen for sample fabrication, and Walter Ching Lee for electronics and circuit design. G.M. thanks Philipp del Hougne, Matthieu Dupré, and Geoffroy Lerosey for helpful discussions. G.M., X.F., and P.S. acknowledge the support of Innovation and Technology Commission of Hong Kong Government through Project ITF/203/15. G.M. and P.S. also acknowledge the support of the Hong Kong Research Grants Council (Grant AoE/P-02/12).

1. Sheng P (2006) *Introduction to Wave Scattering, Localization and Mesoscopic Phenomena* (Springer, Berlin).
2. Mosk AP, Lagendijk A, Lerosey G, Fink M (2012) Controlling waves in space and time for imaging and focusing in complex media. *Nat Photonics* 6:283–292.
3. Rotter S, Gigan S (2017) Light fields in complex media: Mesoscopic scattering meets wave control. *Rev Mod Phys* 89:015005.
4. Vellekoop IM, Mosk AP (2007) Focusing coherent light through opaque strongly scattering media. *Opt Lett* 32:2309–2311.
5. Vellekoop I, Lagendijk A, Mosk A (2010) Exploiting disorder for perfect focusing. *Nat Photonics* 4:320–322.
6. Choi Y, et al. (2011) Overcoming the diffraction limit using multiple light scattering in a highly disordered medium. *Phys Rev Lett* 107:023902.
7. Popoff S, Lerosey G, Fink M, Boccara AC, Gigan S (2010) Image transmission through an opaque material. *Nat Commun* 1:81.
8. Bertolotti J, et al. (2012) Non-invasive imaging through opaque scattering layers. *Nature* 491:232–234.
9. Katz O, Heidmann P, Fink M, Gigan S (2014) Non-invasive single-shot imaging through scattering layers and around corners via speckle correlations. *Nat Photonics* 8: 784–790.
10. Katz O, Small E, Silberberg Y (2012) Looking around corners and through thin turbid layers in real time with scattered incoherent light. *Nat Photonics* 6:549–553.
11. Yu H, Lee K, Park J, Park Y (2017) Ultra high-definition dynamic 3D holographic display by active control of volume speckle fields. *Nat Photonics* 11:186–192.
12. Kaina N, Dupré M, Lerosey G, Fink M (2014) Shaping complex microwave fields in reverberating media with binary tunable metasurfaces. *Sci Rep* 4:6693.
13. Dupré M, del Hougne P, Fink M, Lemoult F, Lerosey G (2015) Wave-field shaping in cavities: Waves trapped in a box with controllable boundaries. *Phys Rev Lett* 115: 017701.
14. Del Hougne P, Lemoult F, Fink M, Lerosey G (2016) Spatiotemporal wave front shaping in a microwave cavity. *Phys Rev Lett* 117:134302.
15. Kuttruff H (2009) *Room Acoustics* (Taylor & Francis, New York).
16. Lyon RH, Dejong RG (2014) *Theory and Application of Statistical Energy Analysis* (Butterworth-Heinemann, Boston).
17. Cummer SA, Christensen J, Alù A (2016) Controlling sound with acoustic metamaterials. *Nat Rev Mater* 1:16001.
18. Ma G, Sheng P (2016) Acoustic metamaterials: From local resonances to broad horizons. *Sci Adv* 2:e1501595.
19. Xu Y, Fu Y, Chen H (2016) Planar gradient metamaterials. *Nat Rev Mater* 1:16067.
20. Yang Z, Mei J, Yang M, Chan NH, Sheng P (2008) Membrane-type acoustic metamaterial with negative dynamic mass. *Phys Rev Lett* 101:204301.
21. Xiao S, Ma G, Li Y, Yang Z, Sheng P (2015) Active control of membrane-type acoustic metamaterial by electric field. *Appl Phys Lett* 106:091904.
22. Ma G, Yang M, Xiao S, Yang Z, Sheng P (2014) Acoustic metasurface with hybrid resonances. *Nat Mater* 13:873–878.
23. Ma G, Yang M, Yang Z, Sheng P (2013) Low-frequency narrow-band acoustic filter with large orifice. *Appl Phys Lett* 103:011903.
24. Yang M, Ma G, Yang Z, Sheng P (2013) Coupled membranes with doubly negative mass density and bulk modulus. *Phys Rev Lett* 110:134301.
25. Akbulut D, Huisman TJ, van Putten EG, Vos WL, Mosk AP (2011) Focusing light through random photonic media by binary amplitude modulation. *Opt Express* 19: 4017–4029.
26. Vellekoop I, Mosk A (2008) Phase control algorithms for focusing light through turbid media. *Opt Commun* 281:3071–3080.
27. Chong YD, Stone AD (2011) Hidden black: Coherent enhancement of absorption in strongly scattering media. *Phys Rev Lett* 107:163901.
28. Nelson PA, Elliott SJ (1991) *Active Control of Sound* (Academic, London).
29. Olson HF, May EG (1953) Electronic sound absorber. *J Acoust Soc Am* 25:1130–1136.
30. Cox TJ, D'Antonio P (2009) *Acoustic Absorbers and Diffusers: Theory, Design and Application* (CRC Press, Boca Raton, FL).
31. Mijić M, Masovic D (2010) Reverberation radius in real rooms. *Telfor J* 2:86–91.